

## Strategies for autonomous rovers at Mars

Martha S. Gilmore,<sup>1</sup> Rebecca Castaño, Tobias Mann, Robert C. Anderson, Eric D. Mjolsness, Roberto Manduchi, R. Stephen Saunders

Jet Propulsion Laboratory, Pasadena, California

**Abstract.** The science return from future robotic exploration of the Martian surface can be enhanced by performing routine processing using onboard computers. This can be accomplished by using software that recognizes scientifically relevant surface features from imaging and other data and prioritizes the data for return transmission to Earth. Two algorithms have been designed and evaluated with field data to identify the properties of the environment that can be reliably detected with onboard imaging and multispectral observation. One algorithm identifies variations in surface textures in images and successfully distinguishes between rocks and soil and between differences in grain size in a rock of a single composition. A second algorithm utilizes a neural net to recognize selected carbonate minerals from spectral reflectance data and successfully identifies carbonates from a set of spectra collected in the field. These types of algorithms will contribute to the efficiency of a landed instrument suite given the limited resources of time, data storage, and available communications opportunities.

### 1. Introduction

NASA has formulated a strategic framework for Mars exploration which emphasizes four themes: (1) the search for life, (2) the understanding of climate history, (3) the identification of resources, and (4) the geological and geophysical history of the planet. The unifying thread between these themes is water, and the identification of past or present locations of water is of paramount importance. The strategy is to first obtain orbital observations of the atmosphere, surface, and interior as currently executed by the Mars Global Surveyor (MGS) and expected from the 2001 Odyssey Orbiter. The second is to characterize selected sites in detail using lander and mobile systems as is planned for the 2003 opportunity. The third step is to land at a site and select samples for return to Earth. Future robotic missions to Mars will also prepare for human exploration. Each of these goals will be enhanced by onboard software that will allow autonomous processing of observational data. The goal of this study is to design software that will provide instrumented rovers with the ability to select and analyze data, characterize the landing site, and test geological hypothesis autonomously.

Future missions to Mars will contain a variety of remote-sensing instruments that complement each other in terms of spatial and spectral resolution. It is of foremost importance that the amount of science return for a given payload be maximized by use of suitable information technology. The problem is how to maximize scientific return given (1) the limited time allocated for the analysis, (2) the limited storage and computing resources of both the lander and the rover, (3) the bandwidth constraints of the downlink channel, and (4) the limited opportunity of interaction with Earth. Current remote science extraction technology is based either on a fixed sequence of operations or

on telerobotics mechanisms. The first case is clearly inefficient; control strategies that respond adaptively to the environment are critical. The second case, telerobotics, is not a viable long-term solution for Mars exploration. In contrast to these two modes of operation, the algorithms described here will enable the science discovery system to have a degree of autonomy, optimizing the overall economy of the information-processing resources of the lander. Since more sophisticated data will be acquired than can be transmitted or stored, the data will have to be analyzed in situ, and the most informative data will be stored or transmitted for analysis, as appropriate. These constraints and the consequent need for onboard algorithms have been observed in rover field tests on the Earth [Arvidson *et al.*, 1998; Stoker, 1998; Pedersen *et al.*, 1999; Arvidson *et al.*, 2000]. The eventual goal of this work is to develop algorithms that can test geologic hypotheses derived from orbital and aerial data sets using data collected by the rover during a mission. The algorithms described here are critical elements of such a system.

The primary goal of this study is to demonstrate a solution to the fundamental problem of getting as much scientifically relevant information as possible returned to scientists on Earth. The key to our solution is to enable a new level of autonomy in the science discovery process by means of onboard data processing and integration. In particular, we are developing onboard visual intelligence sufficient to extract geologically meaningful data from multispectral camera images and spectral reflectance measurements of soil and rock samples and thus to guide the selection, measurement, and return of scientifically important data from significant targets (Figure 1). Using representative sample data, algorithms have been evaluated to identify the useful, feasible properties of the environment that can be reliably detected with the instrumentation available. In this paper, we discuss two approaches. The first approach includes an algorithm that detects subtle variations in surface textures. Using image data collected in the field, we find that identification of texture variations allows the distinction between rocks and soil and between differences in grain size in a rock of a single composition. A second approach uses a neural net to recognize a selected set of spectral reflectance characteristics of individual

<sup>1</sup>Now at Department of Earth and Environmental Sciences, Wesleyan University, Middletown, Connecticut.

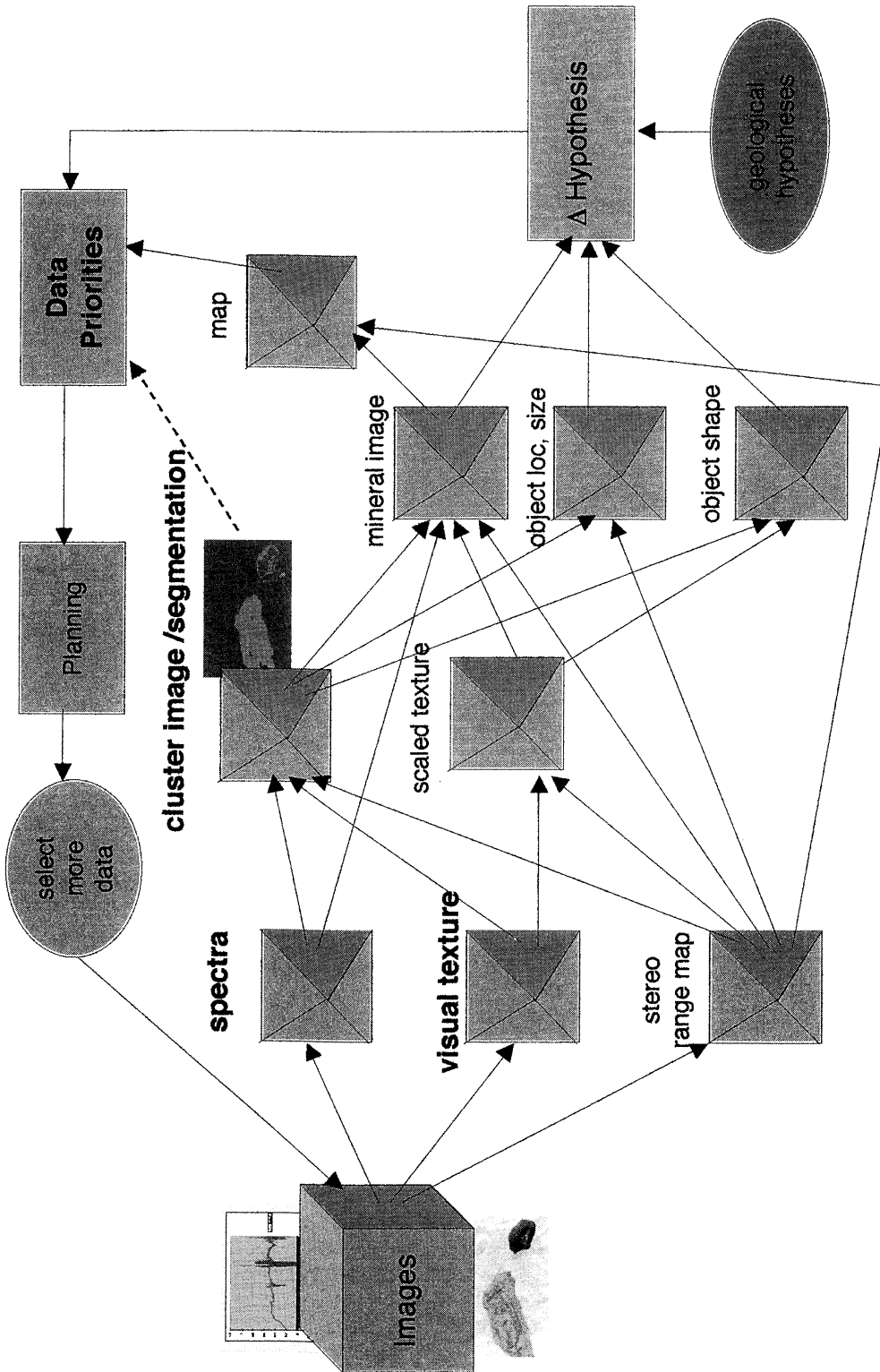


**Figure 1.** Science analysis system flow diagram. Data in the form of images and point spectra collected by the rover are input to algorithms that analyze the spectra, visual texture, and stereo range map. The outputs of these algorithms are then used to generate a clustered image and scaled texture image, which are then used to form a mineral image and determine the location, size, and shape of objects in a scene. Eventually, the extracted information will be used to either confirm or refute the current working geological hypothesis (assumed to be provided by scientists). Prioritization can then be performed for collecting additional data and for transmitting the current data to earth. Modules with a pyramid can be used to analyze data at different scales. Low resolution is useful for a quick overview, while analysis at higher resolutions can provide more details. Bold modules have been implemented. At present, the clustered image is being used to determine data priorities.

rocks. The neural net has been successfully trained on laboratory data to recognize carbonate minerals from a set of unknown reflectance spectra collected in the field. These algorithms will contribute to the full functionality of the lander instrument suite to be developed given the limited resources of time, data storage, downlink data rate, and uplink opportunity.

## 2. Background

### 2.1. Scene Classification by Texture

How does a geologist classify a rock? In the field, geologists assess characteristics such as rock shape, grain size, roundness and sorting, mineralogy, and provenance to allow classification. With the return of images from a multispectral camera, these characteristics can also be inferred on the surface of another planet. To perform geologic analyses on the surface of Mars, the images must be classified into simpler and quantifiable parts that can be identified and processed with an onboard computer. Texture analysis methods have the flexibility to discriminate between distinct objects within an image, they are simple enough to run on the hardware available to a rover, and the state of the art has been advancing steadily in recent years [Unser and Eden, 1989; Malik and Perona, 1990; Popat and Ricard, 1997; De Bonet and Viola, 1998; Manduchi and Portilla, 1999; Malik et al., 1999; Castaño et al., 1999; Manduchi, 2000]. Not only can different types of rocks be distinguished by their texture, but rocks and soils generally have different textures as well, so that texture can be used in a rock detector. Visual texture is an important image property, while geologic texture is a rock property. Although visual texture can be used to indicate geological texture, there is not always an exact correspondence between visual and geologically meaningful texture. The same geologic texture may appear as different visual textures in an image, for example, when two rocks have the same geologic texture and one is near to the camera while the other is farther away. There are also conditions under which two geologic textures may appear as the same visual texture such as a pitted rock in which the pits are distributed similarly to the clasts in another rock. Some of the ambiguities can be removed by performing transforms on the visual texture information to make it independent of scale (distance to camera), illumination angles (time of day and shadows), and phase angle (orientation). The purpose of this study is to assess the utility of texture in autonomous in situ geologic interpretation.

Viking Lander and Pathfinder images reveal that the surface of Mars comprises rocks on the centimeter to meter scales separated by soil and dust [Arvidson et al., 1989; Smith et al., 1997]. We use this type of scene as a model of what to expect for future near-equatorial landed missions at Mars, which presumably have safety requirements similar to the Viking and Pathfinder missions. What does a geologist want to know about the scene? A fundamental distinction is to recognize the difference between rocks and soil. Rocks tell us geologic history and are the focus of both chemical and mineralogical investigations and sample return. The geologist would like to know immediately the variety of rocks in a scene in order to make operational decisions (e.g., the order in which to sample each rock or how many of the instruments to deploy at a given rock). The characteristics of the rocks will dictate which of the geological hypotheses programmed into the rover detection software is selected. Rocks are also potentially hazardous to a rover and impede traversability, and knowledge of their location is thus critical for

traverse planning. Obviously, rock detection is a key desire for rover autonomy.

Once a rock is identified, we next consider which observations can be made that yield clues to the genesis of the rock and the processes that have acted on it through time. Rock shape and rock texture can yield information about the effects of fluvial and aeolian weathering on a rock. Variations in texture, such as pits, flutes, grooves, and linear features, were evident at Pathfinder and used to infer wind direction [Bridges et al., 1999; Greeley et al., 1999]. Pits and rock facets could also be indicative of vesicles and columnar jointing common to volcanic rocks. Linear features could indicate layering due to sedimentary, igneous, or metamorphic processes; likewise, the identification of fragments within a matrix could be indicative of conglomerate, volcanic, or impact breccias [McSween et al., 1999]. The distinction of variations in texture may indicate contacts between protoliths or crusts within a single rock, areas of constant texture such as fields of cobbles, or areas of fine-grained drift. Since the grain size of soils is dependent on aeolian erosion and deposition, texture may prove a useful indicator of the variety of soil deposits. These geologic variations will be considered in our analysis of Mars scenes using texture classification.

### 2.2. Scene Classification by Spectra

Mineralogy derived from spectra is perhaps our most powerful tool for distinguishing targets in a scene. Rock color has been interpreted at both the Pathfinder and Viking lander sites to indicate first-order variations in the degree of dust cover, where downwind rock faces are redder, approaching the color of local soils and drifts [Guinness et al., 1987; McSween et al., 1999]. These redder materials contrast with the darker surfaces of rocks, which are prominent on faces most exposed to erosion; these characteristics lead to the interpretation that the redder portions of the rock are coated by a thin layer of oxidized material [Adams et al., 1986; Guinness et al., 1987; McSween et al., 1999; Bell et al., 2000; Morris et al., 2000]. Two other material color classes were noted for Pathfinder soils and attributed to variations in soil chemistry, grain size, and/or compaction [McSween et al., 1999]. Algorithms that incorporate color and spectral reflectance would provide the ability to quickly assess the distribution of the Pathfinder soils. Likewise, the quick identification of relatively fresh rock surfaces becomes important if they are given high priority for instrument deployment.

The search for life on Mars is highly dependent on aqueous mineralogy. Water is necessary for life on Earth, and there is abundant morphological evidence for the existence of water in the history of Mars [e.g., Parker et al., 1993; Carr, 1996; Head et al., 1999; Malin and Edgett, 2000]. Several terrestrial environments have been identified that indicate the existence of water, provide mechanisms for the preservation and concentration of biologic evidence, and may be associated with detectable mineral assemblages. Evaporite deposits often occur in terrestrial saline lakes and playas and provide rapid mineralization that may entomb microfossils [Walter and Des Maris, 1993]. Hydrothermal systems provide energy to organisms on the Earth's seafloor without the aid of sunlight and are likely to have existed on Mars owing to the presence of large volcanoes and liquid water [e.g., Brakenridge et al., 1985]. The interaction between hydrothermal fluids and country rocks strongly alters the composition of both, which may lead to the precipitation of hydrous minerals and carbonates. Although elusive in the MGS data, the identification of concentrations of

carbonates, sulfides, or other aqueous minerals may be indicative of a hydrothermal system capable of sustaining life. Martian carbonate minerals are also of interest because they have been identified in the Martian meteorites [Clayton and Mayeda, 1988; Middlefehldt, 1994], particularly in ALH84001 coincident with other possible indicators of life [McKay et al., 1996]. It would be advantageous for a rover to have the capability to rapidly detect the occurrence of aqueous minerals, especially if the rover is traversing distances of the order of kilometers and must process a large number of images and spectra. In this study we describe the development of a carbonate detector which can rapidly discern carbonates from reflectance spectra using a neural network, noting that a carbonate detector is being developed independently using a Bayesian classification scheme at Ames Research Center [Roush et al., 1999; Pedersen et al., 1999; Gazis and Roush, 2000].

### 3. Methods: Algorithm development

Visual pattern recognition algorithms allow us to detect significant visual features and to assign the likelihood that a certain area of the image contains geological material of interest. In the basic case presented here, visual pattern recognition consists of a feature extraction step (identification of features of interest) followed by a clustering or segmentation step. Examples of such techniques are color-based discrimination, edge and line detection, morphological processing, two-dimensional shape, and texture segmentation (here listed in increasing order of computational cost). The algorithms are developed and tested using field data with known ground truth information. Algorithm results are scored against the ground truth image interpretation, facilitating improvement of the algorithms. These techniques are now described.

#### 3.1. Texture Algorithm Development and Testing

Our image analysis algorithms consist of essentially two phases. In the first phase the image is measured in various ways (e.g., dn value, spatial information) so that each pixel is associated with several measurements, referred to as a feature vector. Once the feature vectors are obtained, they are examined by a clusterer, which builds a statistical model of the feature vectors and classifies each pixel according to the statistical model. We now elaborate these steps.

Texture is characterized by cyclic intensity variations at different frequencies and orientations. To capture the texture around an image point, a feature vector is constructed in which each element represents the degree to which the local region

exhibits intensity variations of a particular orientation and frequency (period). Feature vectors are formed by first filtering the image with a low-pass Gaussian filter and optionally taking the logarithm of each pixel intensity value. Smoothing the image removes instrument noise, and taking the logarithm of each pixel reduces the effect of spurious pixel intensity differences. After these preprocessing steps we convolve the image with a set of Gabor filters, each of which is sensitive to a different scale and orientation of intensity variations [Daugman, 1985]. The Fourier transform of a Gabor filter is simply a Gaussian function in the frequency domain; a suitably chosen set of Gabor filters can represent the entire image spectrum, i.e., all possible orientations and frequencies in an image. After convolving the image with the set of Gabor filters, a nonlinearity equation is applied to each filter response for each pixel, which transforms the complex valued filter outputs into real numbers. The feature vector associated with each pixel represents the responses of each of the filters in the set centered on that pixel and corresponds to the spectral energy in the neighborhood of the pixel. Each texture will have a different set of spectral frequencies and therefore a different statistical distribution of filter responses. Details of selecting parameters for the Gabor filters are presented by Castaño et al. [1999].

After the feature vectors are formed, they are clustered into several classes representing pixels with similar textures. We model each texture as having a representative feature vector. Measured features are noisy observations centered around the representative class feature, where we have used a Gaussian distribution to model the noise. This texture model is equivalent to representing the texture as an inherently stochastic property described by a Gaussian distribution. Clustering is performed using the expectation-maximization (EM) algorithm to determine the maximum likelihood cluster parameters (mean and covariance for each class) and the class to which each pixel belongs for the set of measured image feature vectors. EM estimates clusters for a fixed number of classes. In some experiments we used Monte Carlo cross validation [Smyth, 1996] to estimate the correct number of classes for an image, while in other experiments we set the number of classes by hand. We discuss selection of the number of classes further in section 4.

There are several parameters other than the number of classes that need to be set in our filterbank/classifier framework. Some parameters control aspects of the system that are readily understandable, such as the scales at which to examine texture features or the particular method used to transform the complex filter outputs into real numbers usable by the classifier. Other parameters are not so intuitive, such as the amount of overlap in



**Figure 2.** (a) Image of pebbles at Silver Lake, California, taken with the Pancam on the FIDO rover. (b) Classified image using the texture algorithm; five classes are identified. (c) Classified image labeled by a geologist; two classes are identified (large pebbles and small pebbles). (d) Classification by texture algorithm setting the number of classes to two and (e) overlain onto the original image. The improved algorithm has been modified to better match the labeling provided by the geologist.

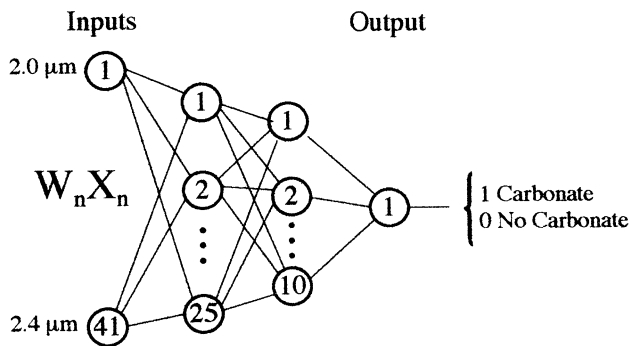


**Figure 3.** Neural network architecture used for carbonate detector. The carbonate detector consists of a neural network with an input layer, two hidden layers, and an output layer. Input signals ( $X_n$ ) are reflectance measurements taken from 2000 to 2400 nm in 10 nm increments. The output is a single node with a binary response. Weight factors ( $W_n$ ) are determined by backpropagation through the neural net; see text for details.

adjacent filters in the filterbank, the region of the frequency domain which the filterbank covers, or classifier parameters such as the number of iterations that the classifier is allowed to run. Both manual and automated methods for determining the optimal parameter settings were investigated. The automated methods were similar to the optimization methods known as simulated annealing and gradient descent [Kirkpatrick *et al.*, 1983]. The attempts to automate parameter selection met with limited success, mostly providing good starting points for the human operator to fine tune the values.

Algorithm performance is measured and validated by comparing results to a geologist's interpretation of the images. That is, the geologist labels a set of images by hand, indicating what geological textures exist in each image. We then both qualitatively and quantitatively compare the algorithm result to this ground truth to determine the degree to which our results agree with the geologist. Figure 2 shows an example image with the regions considered texturally significant to a geologist along with algorithm results for automated and fixed selection of the number classes.

### 3.2. Carbonate Detector

We have developed a method for determining whether or not carbonate minerals are present in a rock based on the sampled reflectance spectra. A neural network is formed from layers of nodes in which each node consists of a linear, weighted combination of the node inputs (reflectance values) followed by a

nonlinear function such as a threshold. The network for the carbonate detector had 41 inputs that represented wavelengths from 2000 to 2400 nm in steps of 10 nm (Figure 3). The input layer was followed by a layer of 25 nodes and then a layer of 10 nodes. A single output indicated if there was a carbonate mineral present or not in the test sample. If the net misidentified the mineral, the weights were adjusted using standard backpropagation until the correct mineral identification was obtained. This trains the network to obtain the desired results. Weight adjustments propagate from the output towards the input layer. The training set is cycled through repeatedly, performing the weight adjustment process for each sample until the output error for the full training set converges to a minimum. The neural net thus recognizes a carbonate spectrum both by absolute values and the slope of the spectrum at each interval and by combinations of these values at different intervals.

The neural network was trained using 10,000 samples of synthetic data. The training data set was constructed using the Advanced Spaceborne Thermal Emission and Reflection Radiometer (ASTER) library (<http://speclib.jpl.nasa.gov/>) of laboratory reflectance spectra of known minerals. Seventeen minerals were used: hematite, magnetite, clinocllore, biotite, albite, quartz, augite, orthoclase, cerussite, strontianite, witherite, calcite, rhodochrosite, siderite, dolomite, azurite, and malachite; the lattermost nine are carbonates. These minerals were chosen to represent the major minerals identified in the rocks at the Silver Lake field site. Gaussian noise with a 2%  $\sigma$  was added to the training data to facilitate comparison of these laboratory spectra to the spectra taken in the field. Sample rock spectra were created in the training data by generating random linear mixtures of the minerals.

After training, the neural net was tested on data collected in the field at Silver Lake, California. Silver Lake Playa is approximately 12 by 3 km and lies 3 km north of Baker, California. Silver Lake has been selected as the test site for the field prototype of the next Mars rover, Field Integration Data and Operations (FIDO). The playa's long-term arid environment, lacustrine features, and sediments [e.g., Enzel *et al.*, 1992] make it a good analog for sites on Mars which may contain evidence of life.

Spectrometer measurements were taken by Ted Roush of NASA Ames using a FieldSpecFR (Analytical Spectral Devices, Inc., ASD) fiberoptic spectrometer operating over the 350-2500 nm wavelength range. This device uses three detectors operating over three wavelength domains. In the 350-1000 nm region a fixed grating is used to disperse the wavelengths across a Si-Photodiode detector array. In the 1000-1800 nm and 1800-2500 nm regions, rotatable gratings are used to disperse the

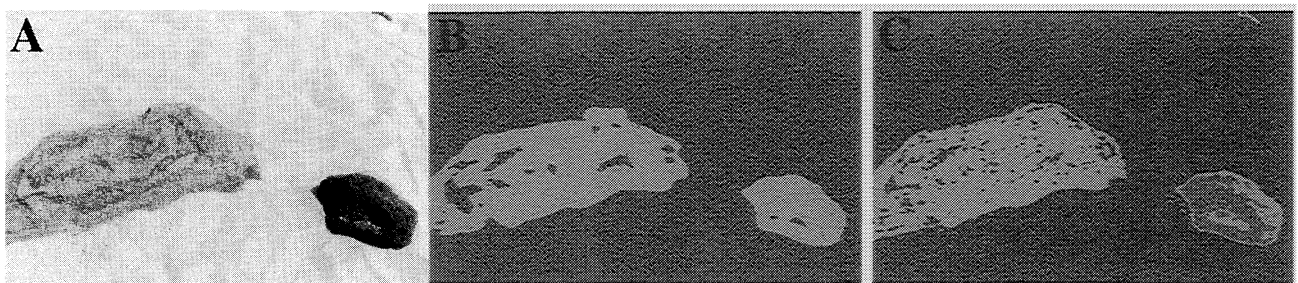


**Figure 4.** (a) Image and classified images set to (b) two and (c) three classes of glassy welded tuff (larger rock) and basalt on sand in the JPL Mars Yard. The large rock is ~0.5 m across. The texture algorithm distinguishes the rocks from the sand.

wavelengths onto InGaAs detectors. Because the instrument was operated without reaching full thermal equilibrium, there are offset differences owing to the response of the various detectors, potentially producing distinct relative reflectance differences for different wavelength regions. A typical data collection sequence consists of measuring the reflectance of a bright, spectrally neutral reference target followed by measurements of the sample of interest. The spectrometer was operated in an automated mode such that the dark current is subtracted from both measurements and the ratio of the sample to reference was calculated for immediate display. The reflectance measurements obtained at the Silver Lake site were made with the fiberoptic cable attached to a 1° field of view foreoptic telescope. Four measurements were collected at each station and averaged. Measurements were taken over a range of distances and azimuths in order to accommodate rock heterogeneity and variations in lighting (see *Gilmore et al.* [1999] for details). The neural net test database comprises 30 field spectra of four different types of rocks. In our experiments on this limited test set, the neural net correctly identified the presence or absence of carbonate minerals in all cases, as discussed in the following section.

## 4. Results

### 4.1. Texture

A variety of field images were selected to evaluate the texture algorithm. As we plan to apply such algorithms on the surface of

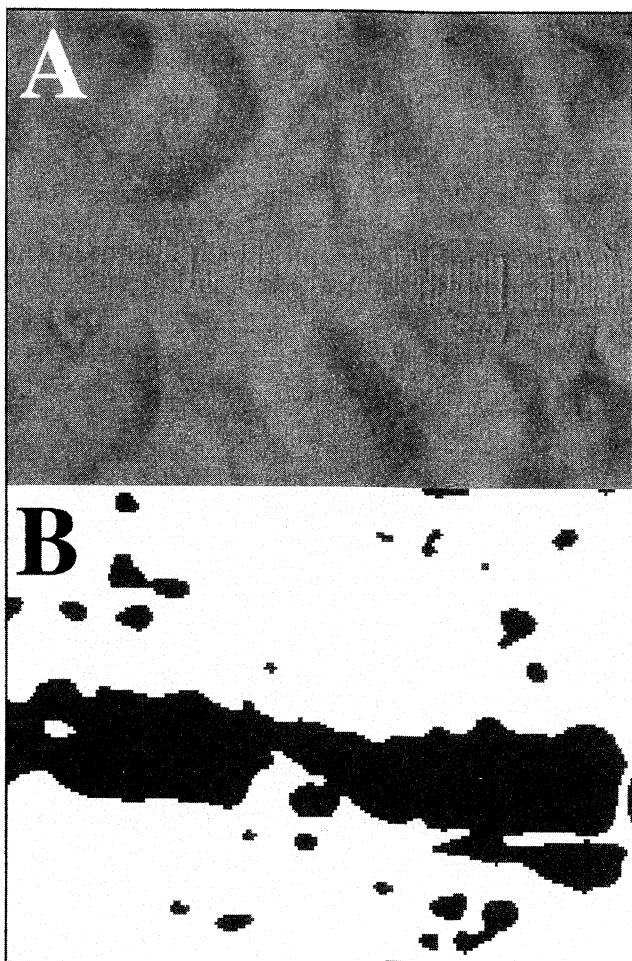


**Figure 5.** (a) Image and (b) classified image of tracks made in sand by the Rocky 7 rover in the JPL Mars Yard. Individual wheel tracks are ~13 cm in diameter.

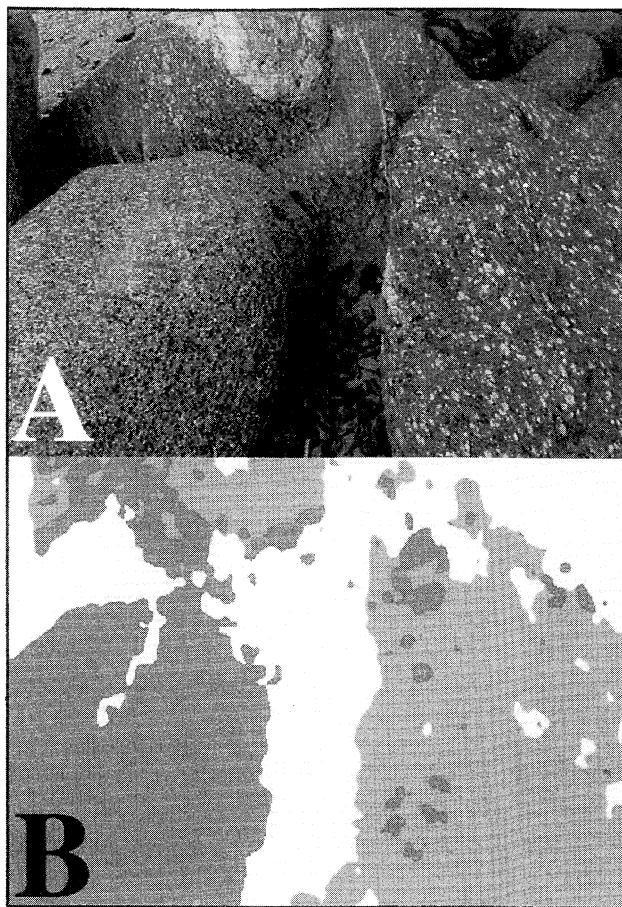


**Figure 6.** (a) Image and (b) classified image of boulders on the floor of Arroyo Seco, which provides some of the water supply for Pasadena, California. The boulders are probably eroded from the Wilson diorite. Although similar mineralogically, the more metamorphosed boulder (right) is distinguished from the unmetamorphosed boulder on the left using a texture algorithm. Image is ~2 m across.

Mars, we began by setting up simple scenes in the Mars Yard at the Jet Propulsion Laboratory (JPL), an outdoor test bed that simulates a Martian landscape. Additional experiments included images taken from the field in the San Gabriel, California, mountains, images taken by the Pancam panoramic imaging system [*Squyres et al.*, 1998] on the FIDO rover during its April 1999 field test at Silver Lake, California [*Arvidson et al.*, 2000], images taken by the IMP camera on Pathfinder, and images taken by the cameras on the Sojourner Truth rover.

**4.1.1. Mars Yard images.** The JPL Mars Yard contains an assortment of rocks of various types and sizes in sand. We set up very simple scenes containing only rocks and quartzose sand for the initial tests of the algorithm. Some results are shown in Figure 4. In this experiment a welded tuff and basalt were placed on the sand, and some sand was added onto the surfaces of the rocks. The true number of textural classes is three: tuff, basalt, and sand. Figure 4b shows the results of the algorithm when the number of classes is set to two. The algorithm correctly separates rock from sand, even distinguishing the sand that lies atop the rocks. If the number of classes is set to three, the algorithm places a portion of the basalt into the third bin. This third class comprises shadowed rock and shadowed sand and reflects the algorithm's inability to detect texture within shadow due to reduction in the dynamic range of the signal. In this scene the

difference in texture between the two rocks is slight, and the algorithm does not accurately detect differences in rock texture. Without specifying the number of classes, the algorithm begins to detect variations in the texture of the sand, but the rocks remain distinct. In such a simple scene the algorithm performs well, mimicking closely the original image.

In a second experiment the algorithm was tested on a scene with uniform composition varying only in texture. The image contained tracks made by the Rocky 7 rover [see *Arvidson et al.*, 1998] in the sand of the Mars Yard (Figure 5). The algorithm successfully distinguished the rover wheel track from the background sand. The linear geometry and orientation of the tracks are evident in the classified image. Such detectors may be useful for identification of linear features in a rock or scene of otherwise similar composition, such as layers [see also *Gulick et al.*, 2000]. This ability could also assist in detection of aeolian features on the rover scale, such as duneforms and wind tails [Greeley *et al.*, 1999], as well the edges of areas of soils with different grain sizes, such as the variation in the drift material and underlying soils observed at the Pathfinder landing site [Moore *et al.*, 1999].

**4.1.2. Field images.** Several images were collected within the local area in order to expand our analysis to natural rock textures. One set of images was obtained in the Arroyo Seco next to JPL, which contain a variety of boulders washed down from the San Gabriel mountains. Figure 6 shows an image containing three large boulders surrounded by smaller rocks and leaves. This texture algorithm was assigned to identify three classes. Examination of Figure 6b shows that the algorithm distinguishes the three boulders from the background. The algorithm then assigns the remaining two classes to the boulders on the basis of grain size, where the larger grain sizes of the rightmost boulder and the quartz vein in the topmost boulder are separated from the

remainder. The mineralogy of the boulders is similar, comprising quartz, feldspar, and pyroxene; thus these boulders would appear similar spectroscopically. The texture algorithm detects variations in grain size due in this case to different degrees of metamorphism, which could go undetected using only a spectrometer.

Variations in grain size are apparent in sandstone of the Vasquez Formation of southern California (Figure 7). The sandstone in this image is a roughly uniform composition where grain size fines toward the bottom of the image. This change is detected by the algorithm, and the classes correspond well with the distribution of grain sizes in the rock. The algorithm is able to detect a contact in a spectrally coherent rock. In this case the contact reflects a change in the carrying capacity of rivers that deposited the sediment.

**4.1.3. FIDO images.** The texture algorithm performs well on images that have relatively large, contiguous areas of texture. Figure 8 includes a pebbly surface at the Silver Lake site, where a path of smaller-diameter grains lies between areas with larger grains. Without an assigned number of classes the algorithm selects four classes, two of which correspond to the smaller grains and two of which correspond to the larger (Figure 8b). This classification identifies the location and orientation of the path. Setting the number of classes to two results in good separation between the smallest-sized pebbles and all other pebbles. The cutoff grain size selected by the algorithm (Figures 8d and 8e) differs from that selected by the geologist (Figure 8c); this can be altered by varying the size of the filters applied to the images. With knowledge of the distance between the camera and the target each filter could be selected to detect actual grain sizes that are deemed important.

The success of the algorithm in detecting grain size differences extends to more complicated images, where a few

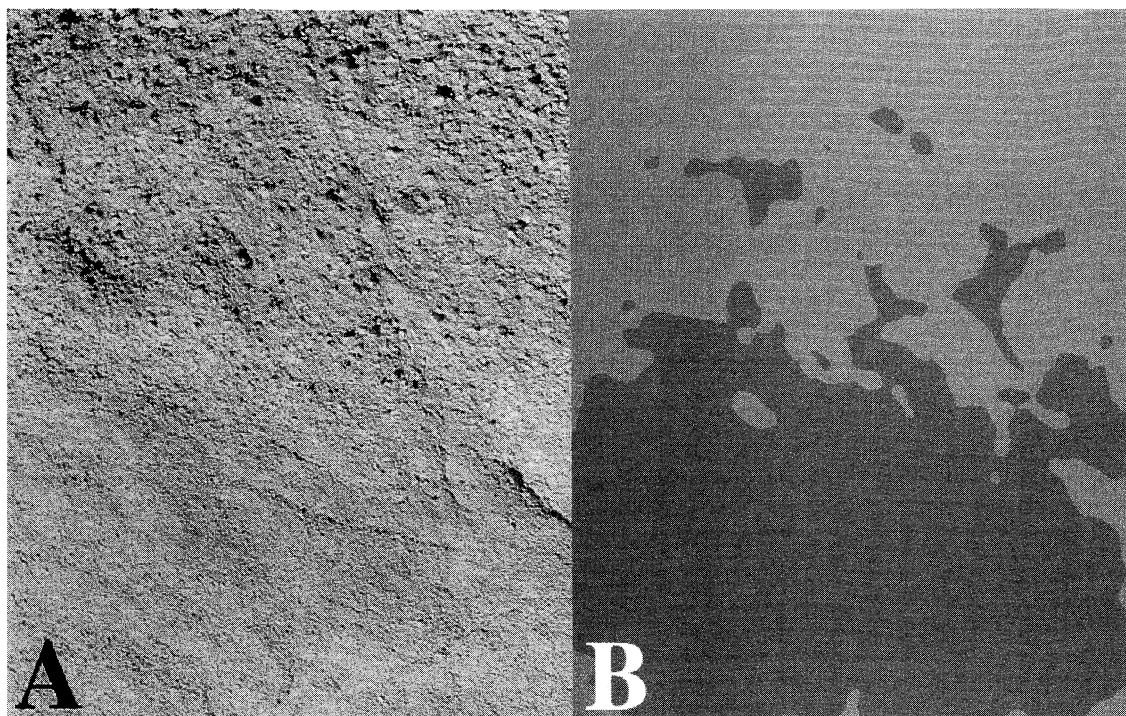


**Figure 7.** (a) Image and (b) classified image of sandstone of the early to mid-Tertiary Vasquez Formation, southern California. Although of similar composition, the transition in grain size is detected by the texture algorithm. Image is ~0.5 m across.



**Figure 8.** (a) Image of pebbly surface at Silver Lake, California taken with the Pancam on the FIDO rover. (b) Classified image using the texture algorithm, number of classes set to four. (c) Classified image labeled by a geologist; two classes are identified. (d) Classification by texture algorithm setting the number of classes to two and (e) overlain onto the original image. Contiguous area of smaller grain size is distinguished from surroundings. Image is <1 m across.

large pebbles lie in a matrix of smaller pebbles. As shown in Figure 9, the algorithm separates the larger pebbles, both light and dark, from the background of smaller-sized clasts. With four classes the algorithm reserves a class that corresponds to the position of the center of the largest pebbles, responding to their relative smoothness (Figure 9b). This information is lost when the number of classes is set to two, reflecting the geologist's desire to simply separate pebbles from matrix.

Similar differences in algorithm versus geologist classification are shown in Figure 10. In this image a hillside comprising darker, larger pebbles abuts an area of lighter colored sand containing a few bushes. The original algorithm classification (Figure 10b) identifies four classes, where the dominant classes correspond to hillside and sand. Although the hillside in reality contains pebbles of a single size range, the algorithm separates the pebbles into two classes of nearer, larger pebbles and pebbles that appear smaller in the image because they are farther away. This problem is common to each image with a perspective view and is the primary motivation for eventually including stereo data that will compensate for distance. The geologist classified the image into three classes, hillside, sand, and bushes (Figure 10c), while the algorithm applied the three classes to large pebbles plus bushes, sand, and sand plus medium-sized grains (Figures 10d and 10e). The geologist's eye was drawn to the stark color differences in this image, which are independent of texture. Similarly, knowing the importance of biota, the geologist assigned the bushes their own class when the sparse bushes often included a pebble signal, causing their visual texture to be less distinct.

The differences between the geologist's labelings and the textural classifications reflect scenes where pertinent scientific questions cannot be addressed by texture alone. In the above examples, color or intensity was a powerful determinant in the detection of geologically interesting materials. Geological experience also resulted in the assignment of a high priority to a minor class (bushes, Figure 10).

**4.1.4. Pathfinder images.** The overall goal of this study is to understand the utility of using texture algorithms on images collected on Mars, and we now focus our investigation on Mars Pathfinder images. In one experiment the texture algorithm was run on an IMP camera image of the rock Chimp with the number of classes set to four (Figure 11). The algorithm does a good job at classifying all of the sunlit portions of Chimp as one class, thus distinguishing it from the remaining rocks and soils in the image. The dark portions of Chimp were grouped with the next largest size rocks in the image, in both the near and far range. This class is, in turn, distinguished from soils. The sky and horizon are correctly identified; however, the smoothest soils are included with the sky class. These results are reproduced in Figure 12. In this scene the rock class includes the soils most disturbed by the Sojourner rover wheels. Less disturbed soils (the white class, Figure 12) are classified independently from smooth soils (dark gray class). Finally, close up and relatively simple views of areas improve the correlation of classes and textures. The rock Mini Matterhorn (Figure 13) and surrounding rocks are texturally distinct, contiguous, and well-lit, which allows the texture classifier to mimic the location and edges of the rock against the soil.



**Figure 9.** (a) Image of centimeter-sized pebbles surface at Silver Lake, California taken with the Pancam on the FIDO rover. (b) Classified image using the texture algorithm, number of classes set to four. (c) Classified image labeled by a geologist; two classes are identified. (d) Classification by texture algorithm with the number of classes set to two and (e) overlain onto the original image. The texture algorithm separates the larger pebbles into a class owing to the fact that they have smoother texture over a continuous area relative to the smaller pebbles.

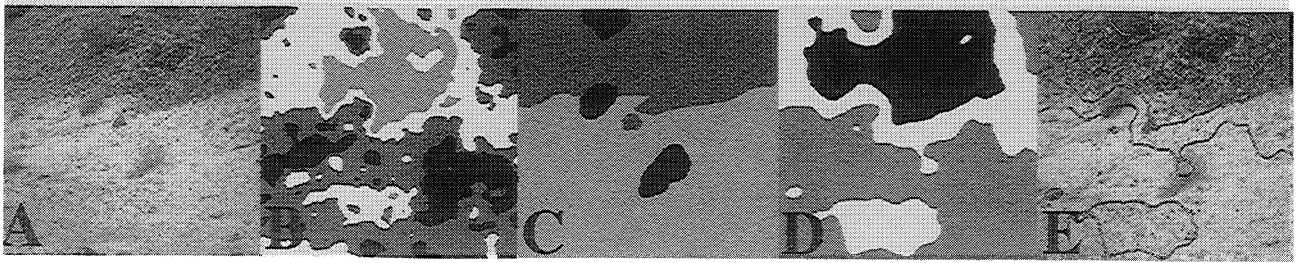


**Figure 10.** (a) Image of rocky slope at Silver Lake, California taken with the Pancam on the FIDO rover. (b) Classified image using the texture algorithm, number of classes set to four. (c) Classified image labeled by a geologist; three classes are identified. (d) Classification by texture algorithm with the number of classes set to three and (e) overlain onto the original image. Areas of larger grain size, including the rocky slope and larger foreground pebbles, are distinguished from sand. Vegetation, important to the geologist, has small textural contrast in this image and is thus ignored by the algorithm. Small bush is <1 m across.

These images from Mars demonstrate the ability of the texture algorithm to classify an image into basic components that correlate generally to rocks and soil. These experiments confirm the ability of images taken on Earth to proxy for images collected at Mars.

#### 4.2. Spectra: Carbonate Detector

Spectra were collected from four rocks that lined a small (~10 m across) outflow channel at the Silver Lake site (Figure 14). The rocks were selected in the field to represent four different lithologic units and were sampled for petrographic analysis.

The rock samples were analyzed with a petrographic microscope and were determined to be granite, limestone, quartz-hornblende gneiss, and a metagabbro. The mineralogies of the rocks are found in Table 1.

Typical spectra for these rocks are shown in Figure 15. Some general features include jumps in the signal at 1000 and 1800 that correspond to the change in the detectors in the instrument. Telluric water vapor has two strong absorptions centered near the 1350-1450 and 1800-1950 nm regions which are omitted for clarity. Weaker water features are sometimes present near 800, 900, and 1150 nm. Calcite (2400 nm), dolomite (2150, 2000, 2350 nm), and talc (2350 nm) absorption features are identifiable in the limestone, while the 540 and 650  $\text{Fe}^{3+}$  charge transfer bands typical of hematite are just visible. The gneiss spectrum is dominated by an absorption feature near 2300 nm attributable to  $\text{Fe}^{2+}$  in hornblende. The granite spectrum displays a hematite absorption at 550 nm. This spectrum also has an absorption at 2400 nm that may be due to biotite but also likely includes clay minerals that are abundant in this highly weathered sample. Identical features in the metagabbro may also be attributed to clays or hornblende present in this sample.

The calcite and dolomite bands visible in the limestone sample are typical of carbonates by having strong absorptions in the 1800–2500 nm portion of the spectrum. This is due to fundamental vibrational modes of the carbonate ion,  $\text{CO}_3^{2-}$  [Hunt and Salisbury, 1971]. The majority of the carbonates are relatively flat in the remainder of the spectrum, except magnesite, siderite, smithsonite, and rhodochrosite, which display absorptions due to the substitution of  $\text{Fe}^{2+}$  or  $\text{Mn}^{2+}$  for  $\text{Ca}^{2+}$  [Hunt and Salisbury, 1971; Gaffey, 1986, 1987]. As the 1800-2500 nm region is so diagnostic of carbonates we chose to focus on this portion of the spectrum. We further reduce the range of study to 2000-2400nm to eliminate the discontinuity due to the

detector and the 1900 nm water band. These discontinuities caused difficulty when the neural net was run on the full spectral range, probably owing to the inconsistent response in the spectra at these wavelengths.

Thirty sample spectra from 2000-2400 nm were selected and used as input to the neural net. After being trained on synthetic spectra, the neural net was successful in separating the 30 spectra into bins of carbonate or noncarbonate (Figures 16a and 16b). The neural net was successful despite variations in the depth of the carbonate band in these field samples, which is the result of variations in lighting geometry and distance of the observation [Gilmore *et al.*, 1999]. The neural net requires 0.1 MB of RAM and the time for testing all 30 spectra samples on a Sun Ultra 60 was ~1 s.

## 5. Discussion

### 5.1. The Utility of Texture

The reader needs only to make a visual inspection of the texture classification images, without other knowledge (e.g., the original image), to realize that texture alone is not a precise indicator of a complex geologic setting. However, the texture results provide important auxiliary information, which, when combined with other data such as color and stereo, may help address geologic questions autonomously. Several strengths of the texture classifier are listed below.

**5.1.1. Rock detection.** While the algorithm tends to overclassify images, the largest of the classes often corresponds with texturally distinct features. The success rate is higher if the classes are contiguous areas of similar texture. Since rocks differ significantly from soils, this results in successful detection of individual rocks from the background in Mars-like environments (Mars Yard and Pathfinder results). In the desert pavement environment of the Silver Lake site the algorithm instead distinguished contiguous areas of common grain size. In practice, rock detection by the texture algorithm would be enhanced in a Mars Yard type environment by setting the number of classes to two (or three, including the sky), which emphasizes the stark textural differences in a terrain (e.g., Figure 4b).

**5.1.2. Textural variation.** Perhaps the most powerful use of texture is when examining rocks or soils of similar composition but different grain size (Figures 5-7). This may be important on Mars, where ferric and ferrous dust coatings are seen on rocks of all sizes at the Pathfinder landing site [McSween *et al.*, 1999].

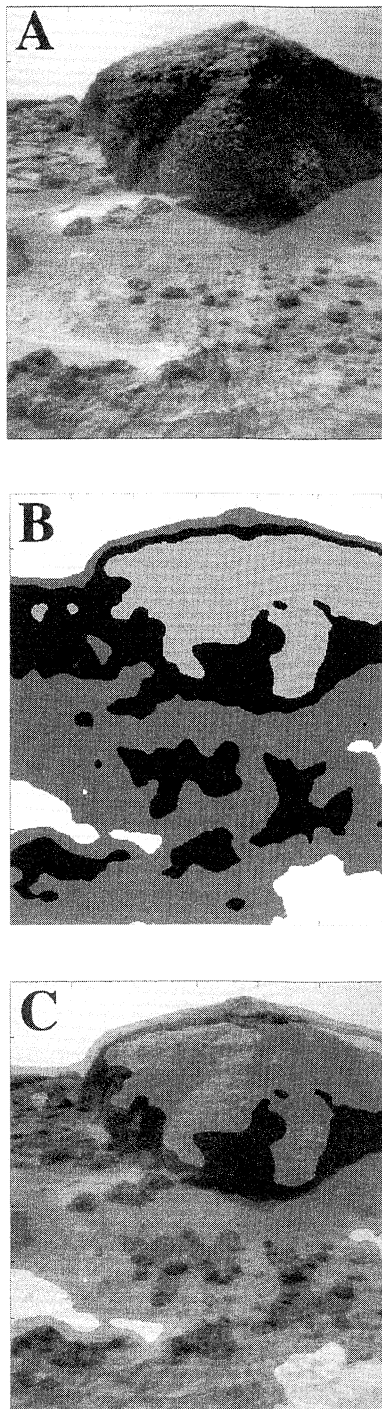


**Figure 11.** (a) Imager for Mars Pathfinder (IMP) camera image of rock Chimp and environs. Chimp is 39 cm tall. Portion of public release image PIA00963. (b) Texture results for image, number of classes set to four. (c) Overlay of Figure 11a and 11b. The texture classifier does well to separate Chimp from the remainder of the image and correctly identifies the sky.

Autonomous textural classification of a scene may distinguish rock with pits, grooves, and flutes which may have priority as indicators of igneous origin, aeolian activity, and weathering [Bridges *et al.*, 1999], fluvial modification [Basilevsky *et al.*, 1999], sedimentation [Rover Team, 1997], or other processes. Texture may serve as a useful discriminant between soils. Many

of the smooth Pathfinder soils are located behind rocks as wind tails (e.g., Figure 11) or in duneforms; both types of deposits are interpreted as aeolian and indicative of local wind direction [Smith *et al.*, 1997; Greeley *et al.*, 1999]. These features are consistent with wind directions inferred from the smooth (dusty) sides of rocks [McSween *et al.*, 1999]. Identification of the smoothest textures in a scene may correspond to the above features and indicate prevailing wind direction.

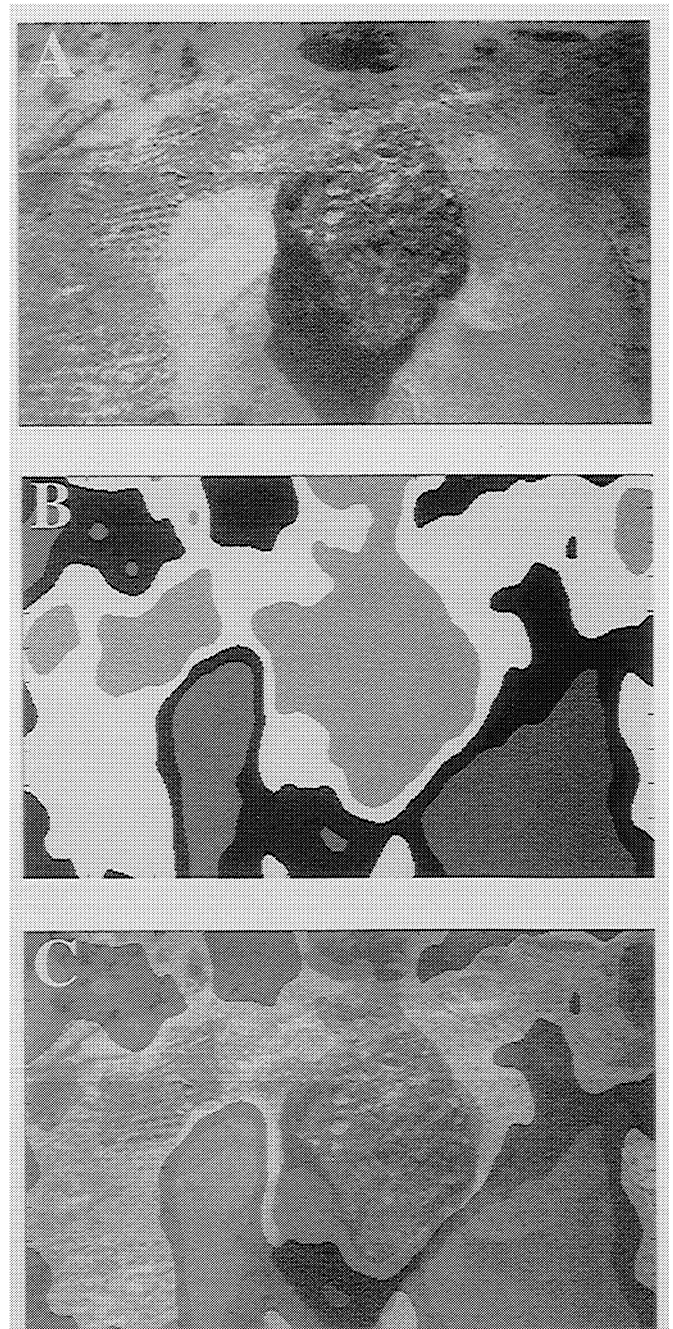


**Figure 12.** (a) Sojourner rover camera image of area near lander, including rocks, undisturbed soils, and soils disturbed by the rover wheels. Rover wheel diameter is 7 cm. Portion of PIA00673. (b) Texture results for image, number of classes set to four. (c) Overlay of Figures 12a and 12b. The texture algorithm combines the rock with the rough soil produced by the rover wheels. Smooth soil areas are grouped together.

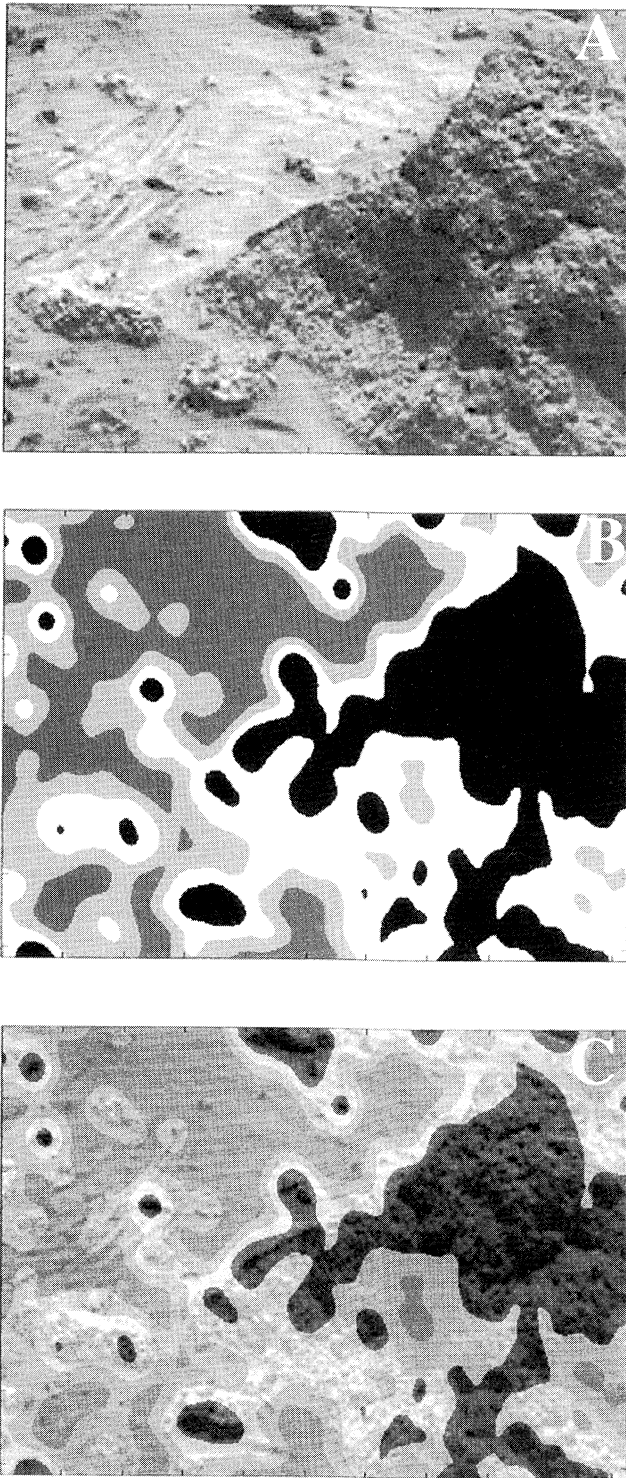


**Figure 13.** (a) IMP camera super resolution image of Mini Matterhorn. Grooves in the left portion of the image were formed from the lander airbags. Image is  $\sim 1$  m across. Portion of PIA00817. (b) Texture results for image, number of classes set to four. (c) Overlay of Figures 13a and 13b. The white and black classes correspond well with Mini Matterhorn and nearby rocks of similar texture.

**5.1.3. Site variability.** While it is difficult to assess texture results without secondary information, the texture algorithm does allow the distribution and quantification of texture variability within a scene. With this capability the rover can collect a low-

resolution image of a scene, classify the image according to texture, and collect a high-resolution image of each of the identified textures for downlink to Earth. This representative sampling of the scene can be used to plan subsequent investigations without collecting a high-resolution panorama at each rover waypoint. The texture classification also allows the identification of the areal extent of various textural units, where one might want to select the most rare unit for initial investigation. This becomes important as images are collected from a moving platform, allowing the rapid identification of textures that have not yet been sampled.

## 5.2. Specified Targets: Carbonate Detection

The success of the neural net at discriminating carbonates from noncarbonates using field spectra makes it a potentially powerful tool for integration onto future Mars payloads. However, the success was predicated on the carbonate features being distinct from the noncarbonate features in the 2000-2400 nm portion of the spectrum. The inclusion of jumps in the spectra due to the detector and water bands caused the neural net to fail when it analyzed data over the full 400-2500 nm range. This may be due to the fact that the jumps were not consistent from one spectrum to the next and had a random effect on the outcome for each run. We predict that a more complex neural net could learn that assigning less weight to these portions of the spectrum would result in the correct answer. In practice, it would be relatively simple to exclude noisy portions of the spectrum due to the Martian atmosphere from the neural net input.

Several types of minerals have been identified as high priority on Mars and will be considered in the further development of the neural net algorithm. Evaporite minerals, such as phosphates, carbonates, and sulfates, are deposited by water and are uniquely suited to entomb the contents of the water column, including life. Hydrous minerals such as amphibole and clays offer the possibility of water extraction for future human missions. Airborne quartz particles present a danger to astronauts as they cannot be expelled from the lungs and result in silicosis. Very fine-grained clay minerals may pose significant risks to machinery and filtering systems that can hamper the human effort at Mars.

## 5.3. Relevance to Future Mars and Human Missions

**5.3.1. A mission scenario.** The texture and spectral results described here can be integrated into a payload that processes the sensors' output, takes control of the instruments, and selects the appropriate information to send to Earth. More specifically, it functions as an automatic attention-focusing system, designed to cut efficiently through the Gordian knot of too much instrument data and too little downlink bandwidth. A simple task sequence to be performed by the a rover equipped with these algorithms is outlined in the following:

**Table 1.** Mineralogy for Sampled Rocks

Rock	Mineralogy <sup>a</sup>
Granite	orthoclase, quartz, albite, biotite, ilmenite, magnetite, apatite, sphene
Limestone	calcite, dolomite, hematite, talc
Gneiss	quartz, orthoclase, hornblende, biotite, minor garnet (grossular), apatite, sphene, oxide
Metagabbro	hornblende, diopside, anorthite, orthoclase, magnetite, sphene

<sup>a</sup>In order of relative abundance

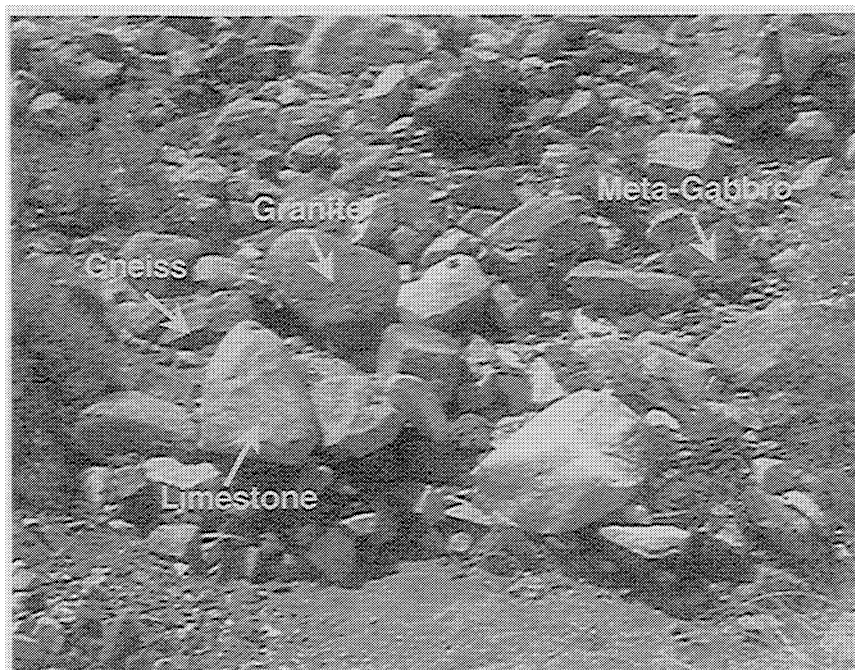


**Figure 14.** Outcrop at Silver Lake field site, including four rocks from which spectra were collected. Limestone is ~0.5 m in width.

1. Autonomous software feeds each low-resolution image to a computer on board the lander.
2. The system scans each image, automatically decomposes it into segments according to visual cues such as shape, edges and visual texture.
3. Each image segment is autonomously classified according to its likelihood for containing important textural variations or novel mineralogy, given all the available background and contextual information.
4. The resulting class information is fed to onboard planning

and scheduling software, which can operate in one of two modes: fully autonomous mode generates a sequence of commands to autonomously direct the camera to image selected parts of the target at higher resolution; semiautonomous mode flags high-priority images, downlinks them to Earth, then receives and executes scientists' instructions for target selection and the deployment of instrumentation.

The same procedure can be applied iteratively across a number of scales to investigate targets systematically at ever-increasing resolution. The scenario described constitutes an adaptation of

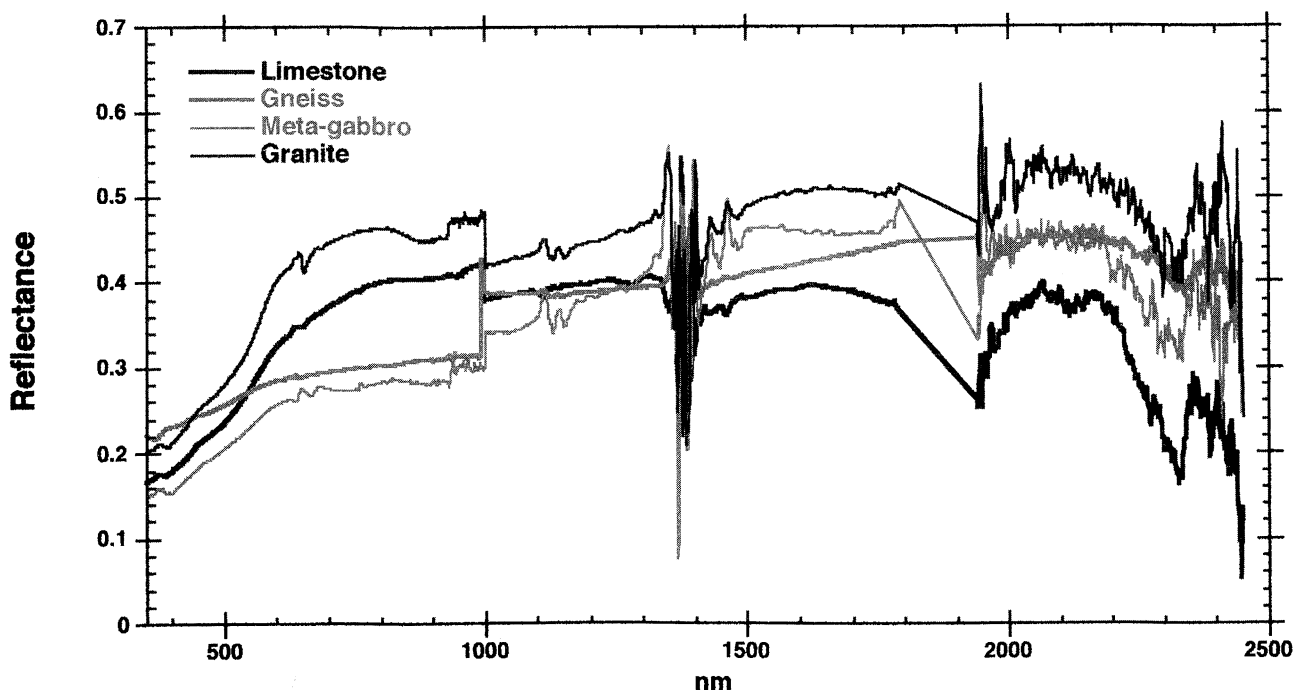


**Figure 15.** Reflectance spectra of four rocks indicated in Figure 14 and described in Table 1. See text for details. Water absorptions are omitted for clarity.

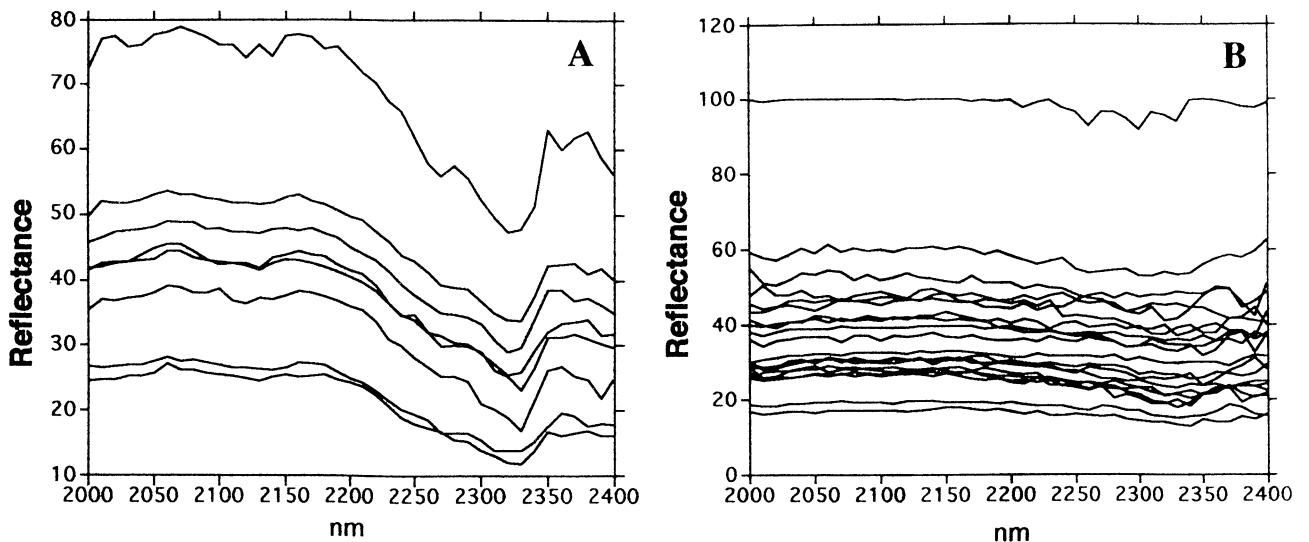


**Figure 16.** Results of carbonate detector on the 2000-2400 nm region of 30 field spectra collected at the Silver Lake site (Figure 15). The absorption at  $\sim 2330$  nm present in each of (a) the carbonate spectra allowed them to be successfully distinguished from (b) non-carbonate spectra by the neural net. Notice the difference in scale on the ordinate of the two graphs.

prior work in which we have integrated planning and scheduling with automated data collection directed toward maximizing scientific return [Estlin, *et al.*, 1999].

**5.3.2. Data rate triage.** Autonomous onboard science processing not only can help increase the efficiency of the science discovery process but also can contribute to optimizing the use of available communications resources. Imaging and multispectral instruments placed on future Mars rovers can produce vast loads of information which may quickly saturate the limited capacity of the downlink channel. Data compression must be used to reduce the size of the data to be transmitted. Unfortunately, traditional data compression techniques are “content blind,” in the sense that they are unaware of the scientific importance of different parts of the image being compressed. By making use of the information provided by the onboard visual classifiers, we may design compression algorithms that preserve high resolution and accuracy in “important” regions of an image (e.g., areas with high likelihood of containing carbonates) and larger quantization errors in “less important” regions (e.g., sky or uniform sand). A simple way to achieve this goal is by means of a “prioritized buffer,” where data segments are ordered according to their scientific value [Manduchi *et al.*, 2000]. This guarantees that high-priority data segments are transmitted before low-priority data segments and that in case of buffer overflow (due to limited storage resources or downlink channel capacity) only the lower-priority segments are discarded.

**5.3.3. Applications to human exploration.** We believe that our mechanism for autonomous science discovery can be developed further to ultimately assist humans in delicate and critical operations. Human exploration of Mars will benefit immensely by augmented reality systems that can help the operator perform science-directed tasks. These algorithms will allow the possibility of using head-up displays in which magnified images are automatically segmented and displayed to astronauts, with visual markers indicating the most promising targets for high-resolution imaging. Astronauts will use this analysis to focus their energies on promising pursuits, thereby increasing their efficiency. An astronaut will have limited time

to devote to scientific experiments, monitoring of instruments, and analysis of data. The relevant signatures may be very small. For example, if a biomarker is observable in a 100X image and a rock surface is 15cm x 15cm, it will require  $\sim 10^4$  images to inspect the surface. An analysis algorithm can look at all of the images and select the most interesting 100 for the human to study. At 10% coverage of each sample the same hundredfold reduction of information would permit detailed examination of 10 samples per execution. Without the analysis and prioritization algorithm the astronaut must randomly select sections of the surface to study and could easily miss important targets.

Autonomous systems will also be invaluable components of rovers that both precede the arrival of humans and assist them when they arrive. Future rovers will likely perform long-range (tens to hundreds of kilometers from the outpost) reconnaissance sorties. The algorithms we propose to develop can be used by these rovers to autonomously search for selected minerals that may be utilized for resources (aqueous minerals), assess and identify hazards (quartz particles, fine dust, variations in traversability), and search for biomarkers or biologic activity. In the realm nearer to the outpost (10 km radius), rovers could rapidly flag targets of interest for the astronauts to visit and investigate further [Cabrol *et al.*, 1999]. Such smart rovers may operate continuously, saving the astronauts valuable time and exposure. This speaks directly to an assumption addressed in the Mars Human Reference Mission (pp. 3-12) that astronauts will “[r]ely on reasonable advances in automation to perform a significant amount of the routine activities throughout the mission.” Additionally, the Reference Mission specifies that crew operations depend upon (pp. 1-24) “[h]ighly reliable, autonomous system operations...without intensive crew participation.” The algorithms investigated here are a fundamental step towards producing reliable, autonomous systems for human exploration.

## 6. Conclusions

We find that the textural classification of rocks provides important auxiliary information about a scene that can be utilized

by a landed system. The texture algorithm met with greatest success when the textural variations between objects of interest were most distinct, such as between rocks and soil, between disturbed and undisturbed soils, and between rocks with different grain sizes. These distinctions were enhanced when the algorithm was limited to detecting a small number of classes. The neural net performed well to distinguish carbonate minerals in rocks collected in the field. This is due to the distinctiveness of the carbonate absorption band in a selected portion of the spectrum. Future development of the detector to include other minerals and mixtures of minerals will test the reliability of this technique. The results of this work demonstrate the validity and utility of onboard processing of data in the future exploration of Mars as well as computational field geology techniques in general.

**Acknowledgments.** We thank Ted Roush, Ed Guinness, and Brian Ebel for field instrumentation and assistance in the collection of the images and spectra from Silver Lake. Ray Arvidson provided a helpful review and kindly provided images taken by the FIDO rover during its April 1999 field test; additional information can be found at <http://wufs.wustl.edu/rover>. Richard Maclin and Benjamin Bornstein contributed to the development of the neural net training code. Discussions with Ginny Gulick and Paul Gazis were appreciated and helpful. Thanks also to Jim Greenwood for petrographic assistance. This work was sponsored by a grant from the CalTech/JPL Technology and Applications Programs to R.S.S., by the NASA Autonomy Program, and by the NASA Remote Exploration and Experimentation (REE) Program and was carried out at the Jet Propulsion Laboratory, California Institute of Technology, under a contract with the National Aeronautics and Space Administration.

## References

- Adams, J. B., M. O. Smith, and P. E. Johnson, Spectral mixture modeling: A new analysis of rock and soil types at the Viking Lander 1 site, *J. Geophys. Res.*, *91*, 8098-8112, 1986.
- Arvidson, R. E., J. L. Gooding, and H. J. Moore, The Martian surface as imaged, sampled, and analyzed by the Viking Landers, *Rev. Geophys.*, *27*, 39-60, 1989.
- Arvidson, R. E., et al., Rocky 7 prototype Mars rover field geology experiments, I, Lavic Lake and Sunshine Volcanic Field, California, *J. Geophys. Res.*, *103*, 22,671-22,688, 1998.
- Arvidson, R. E., et al., Students participate in Mars Sample Return Rover field tests, *EOS Trans. AGU*, *81*, 113-117, 2000.
- Basilevsky, A. T., W. J. Markiewicz, N. Thomas, and H. U. Keller, Morphologies of rocks within and near the Rock Garden at the Mars Pathfinder landing site, *J. Geophys. Res.*, *104*, 8617-8636, 1999.
- Bell, J. F., III, et al., Mineralogic and compositional properties of the Martian soil and dust: Results from Mars Pathfinder, *J. Geophys. Res.*, *105*, 1721-1755, 2000.
- Brakenridge, G. R., H. E. Newsom, and V. R. Baker, Ancient hot springs on Mars: Origins and paleoenvironmental significance of small Martian valleys, *Geology*, *13*, 859-862, 1985.
- Bridges, N. T., R. Greeley, A. F. C. Haldemann, K. E. Herkenhoff, M. Kraft, T. J. Parker, and A. W. Ward, Ventifacts at the Pathfinder landing site, *J. Geophys. Res.*, *104*, 8595-8615, 1999.
- Cabrol, N. A., J. J. Kosmo, R. C. Trevino, and C. Stoker, Astronaut-rover interaction for planetary surface exploration: '99 Silver Lake first ASRO experiment, *Lunar Planet. Sci.*, [CD-ROM], XXX, abstract 1069, 1999.
- Carr, M. H., *Water on Mars*, Oxford Univ. Press, New York, 1996.
- Castaño, R., T. Mann, and E. Mjolsness, Texture analysis for Mars rover images, in *Applications of Digital Image Processing XXII, Proc. SPIE Int. Soc. Opt. Eng.*, 3808, 162-173, 1999.
- Clayton, R. N., and T. K. Mayeda, Isotopic composition of carbonate in EET79001 and its relation to parent body volatiles, *Geochim. Cosmochim. Acta*, *52*, 925-927, 1988.
- Daugman, J. G., Uncertainty relation for resolution in space, spatial frequency, and orientation optimized by two-dimensional visual cortical filters, *J. Opt. Soc. Am. A Opt. Image Sci.*, *2*, 1160-1169, 1985.
- De Bonet, J. S., and P. Viola, Texture recognition using a non-parametric multi-scale statistical model, in *Conference Computer Vision and Pattern Recognition (CVPR'98)*, pp. 641-647, Inst. Electr. and Electron. Eng., New York, 1998.
- Enzel, Y., W. J. Brown, R. Y. Anderson, L. D. McFadden, and S. G. Wells, Short-duration Holocene lakes in the Mojave River drainage basin, southern California, *Quat. Res.*, *38*, 60-73, 1992.
- Estlin, T., A. Gray, T. Mann, G. Rabideau, R. Castaño, S. Chien, and E. Mjolsness, An integrated system for multi-rover scientific exploration, in *Proceedings of the 16th National Conference on Artificial Intelligence (AAAI-99)*, pp. 613-620, AAAI Press, Menlo Park, California, 1999.
- Gaffey, S. J., Spectral reflectance of carbonate minerals in the visible and near infrared (0.35-2.55  $\mu\text{m}$ ): Calcite, aragonite, and dolomite, *Am. Mineral.*, *71*, 151-162, 1986.
- Gaffey, S. J., Spectral reflectance of carbonate minerals in the visible and near infrared (0.35-2.55  $\mu\text{m}$ ): Anhydrous carbonate minerals, *J. Geophys. Res.*, *92*, 1429-1440, 1987.
- Gazis, P. R., and T. L. Roush, Autonomous identification of carbonates using near-IR reflectance spectra during the February 1999 Marsokhod field tests, *J. Geophys. Res.*, in press, 2000.
- Gilmore, M. S., R. Castaño, T. Roush, E. Mjolsness, T. Mann, R. S. Saunders, B. Ebel, and E. Guinness, Effects of distance and azimuth on spectroscopic measurements at Silver Lake, CA, *Lunar Planet. Sci. [CD-ROM]*, XXX, abstract 1886, 1999.
- Greeley, R., M. Kraft, R. Sullivan, G. Wilson, N. Bridges, K. Herkenhoff, R. O. Kuzmin, M. Malin, and W. Ward, Aeolian features and processes at the Mars Pathfinder landing site, *J. Geophys. Res.*, *104*, 8573-8584, 1999.
- Guinness, E. A., R. E. Arvidson, M. A. Dale-Bannister, R. B. Singer, and E. A. Bruckenthal, On the spectral reflectance properties of materials exposed at the Viking landing sites, *Proc. Lunar Planet. Sci. Conf. 17th, Part 2, J. Geophys. Res.*, *92*, suppl., E575-E587, 1987.
- Gulick, V. C., R. L. Morris, M. A. Ruzon, and T. L. Roush, Autonomous image analysis during the 1999 Marsokhod rover field test, *J. Geophys. Res.*, in press, 2000.
- Head, J. W., III, H. Hiesinger, M. A. Ivanov, M. A. Kreslavsky, S. Pratt, and B. J. Thomson, Possible ancient oceans on Mars: Evidence from Mars Orbiter Laser Altimeter data, *Science*, *286*, 2134-2137, 1999.
- Hunt, G. R., and J. W. Salisbury, Visible and near-infrared spectra of minerals and rocks, II, Carbonates, *Mod. Geol.*, *2*, 23-30, 1971.
- Kirkpatrick, S., C. D. Gelatt Jr., and M. P. Vecchi, Optimization by simulated annealing, *Science*, *220*, 671-680, 1983.
- Malik, J., and P. Perona, Preattentive texture discrimination with early vision mechanisms, *J. Opt. Soc. Am. A Opt. Image Sci.*, *7*, 923-932, 1990.
- Malik, J., S. Belongie, J. Shi, and T. Leung, Textons, contours and regions: Cue integration in image segmentation, in *7th International Conference on Computer Vision (ICCV'99)*, pp. 918-925, Inst. of Electr. and Electron. Eng., New York, 1999.
- Malin, M. C., and K. S. Edgett, Evidence for recent groundwater seepage and surface runoff on Mars, *Science*, *288*, 2330-2335, 2000.
- Manduchi, R., Mixture models and the segmentation of multimodal textures, in *IEEE Conference on Computer Vision and Pattern Recognition (CVPR2000)*, pp. 1-98-1-104, Inst. of Electr. and Electron. Eng., New York, 2000.
- Manduchi, R., and J. Portilla, Independent component analysis of textures, in *7th International Conference on Computer Vision (ICCV'99)*, pp. 1054-1060, Inst. of Electr. and Electron. Eng., New York, 1999.
- Manduchi, R., S. Dolinar, F. Pollara, and A. Matache, Onboard science processing and buffer management for intelligent deep space communications, paper presented at IEEE Aerospace Conference, Big Sky, Mont., March 2000.
- McKay, D. S., E. Gibson, K. Thomas-Keptra, V. Hogatollah, C. Romanek, S. Clemett, S. Chiller, C. Maechling, and R. Zare, Search for past life on Mars: Possible relic biogenic activity in Martian meteorite ALH84001, *Science*, *273*, 924-930, 1996.
- McSween, H. Y., et al., Chemical, multispectral, and textural constraints on the composition and origin of rocks at the Mars Pathfinder landing site, *J. Geophys. Res.*, *104*, 8679-8715, 1999.
- Middlefehldt, D. W., ALH84001: A cumulate orthopyroxenite member of the Martian meteorite class, *Meteoritics*, *29*, 214-221, 1994.
- Moore, H. J., D. B. Bickler, J. A. Crisp, H. J. Eisen, J. A. Gensler, A. F. C. Haldemann, J. R. Matijevic, L. K. Reid, and F. Pavlics, Soil-like deposits observed by Sojourner, the Pathfinder rover, *J. Geophys. Res.*, *104*, 8729-8746, 1999.

- Morris, R. V., et al., Mineralogy, composition, and alteration of Mars Pathfinder rocks and soils: Evidence from multispectral, elemental, and magnetic data on terrestrial analogue, SNC meteorite, and Pathfinder samples, *J. Geophys. Res.*, *105*, 1757-1817, 2000.
- Parker, T. J., D. S. Gorsline, R. S. Saunders, D. C. Pieri, and D. M. Schneeberger, Coastal geomorphology of the Martian northern plains, *J. Geophys. Res.*, *98*, 11,061-11,078, 1993.
- Pedersen, L., S. Apostolopoulos, W. Whittaker, W. Cassidy, P. Lee, and T. Roush, Robotic rock classification using visible light reflectance spectroscopy, *Lunar Planet. Sci.*, [CD-ROM], *XXX*, abstract 1340, 1999.
- Popat, K., and R. Picard, Cluster-based probability model and its application to image and texture processing, *IEEE Trans. Image Proc.*, *6*, 268-284, 1997.
- Roush, T. L., et al., Autonomous science decision making for Mars sample return *Lunar Planet. Sci.*, [CD-ROM], *XXX*, abstract 1586, 1999.
- Rover Team, Characterization of the Martian surface deposits by the Mars Pathfinder rover, Sojourner, *Science*, *278*, 1765-1768, 1997.
- Smith, P. H., et al., Results from the Mars Pathfinder Camera, *Science*, *278*, 1758-1765, 1997.
- Smyth, P., Clustering using Monte Carlo Cross-Validation, in *Proceedings of the Second International Conference on Knowledge Discovery and Data Mining (KDD-96)*, pp. 126-133, MIT Press, Cambridge, Massachusetts, 1996.
- Squyres, S. W., et al., The Athena Mars rover science payload, *Lunar Planet. Sci.*, [CD-ROM], *XXIX*, abstract 1101, 1998.
- Stoker, C., The search for life on Mars: The role of rovers, *J. Geophys. Res.*, *103*, 28,557-28,575, 1998.
- Unser, M., and M. Eden, Multiresolution feature extraction and selection for texture segmentation, *IEEE Trans. Patt. Anal. Mach. Intell.*, *2*, 717-728, 1989.
- Walter, M. W., and D. J. Des Marais, Preservation of biological information in thermal spring deposits: Developing a strategy for the search for a fossil record on Mars, *Icarus*, *101*, 129-143, 1993.
- 
- R. C. Anderson, R. Castaño, R. Manduchi, T. Mann, E. D. Mjolsness, and R. S. Saunders, Jet Propulsion Laboratory, 4800 Oak Grove Drive, Pasadena, CA 91109. (robert.anderson@jpl.nasa.gov; rebecca.castano@jpl.nasa.gov; roberto.manduchi@jpl.nasa.gov; tobias.mann@jpl.nasa.gov; eric.mjolsness@jpl.nasa.gov; saunders@jpl.nasa.gov)
- M. S. Gilmore, Department of Earth and Environmental Sciences, Wesleyan University, 265 Church Street, Middletown, CT 06459. (mgilmore@wesleyan.edu)

(Received April 24, 2000; revised August 23, 2000; accepted September 12, 2000.)